

Comparison-based Image Quality Assessment for Parameter Selection

Haoyi Liang, *Student Member, IEEE*, and Daniel S. Weller, *Member, IEEE*

Abstract—Image quality assessment (IQA) is traditionally classified into full-reference (FR) IQA and no-reference (NR) IQA according to whether the original image is required. Although NR-IQA is widely used in practical applications, room for improvement still remains because of the lack of the reference image. Inspired by the fact that in many applications, such as parameter selection, a series of distorted images are available, the authors propose a novel comparison-based image quality assessment (C-IQA) method. The new comparison-based framework parallels FR-IQA by requiring two input images, and resembles NR-IQA by not using the original image. As a result, the new comparison-based approach has more application scenarios than FR-IQA does, and takes greater advantage of the accessible information than the traditional single-input NR-IQA does. Further, C-IQA is compared with other state-of-the-art NR-IQA methods on two widely used IQA databases. Experimental results show that C-IQA outperforms the other NR-IQA methods for parameter selection, and the parameter trimming framework combined with C-IQA saves the computation of iterative image reconstruction up to 80%.

Index Terms—Image distortion, image quality assessment (IQA), human visual system (HVS), comparison-based image quality assessment (C-IQA), parameter selection

I. INTRODUCTION

Obtaining an image with high perceptual quality is the ultimate goal of many image processing problems, such as image reconstruction, denoising and inpainting. However, measuring the perceptual image quality by subjective experiment is time-consuming and expensive, so designing an image quality assessment (IQA) algorithm that agrees with the human visual system (HVS) [1]–[5] is a foundational image processing objective. Moreover, most image restoration algorithms require one or more parameters to regulate the restoration process, and no-reference IQA methods can be used to guide selecting the parameters. For instance, the regularization parameter of image reconstruction [6] is selected by a no-reference image quality index [7]. However, most existing no-reference IQA algorithms output the estimated image quality based on a single distorted image, ignoring that different degraded images can provide more information together to the quality estimation of each degraded image. This observation inspires us to develop a comparison-based IQA method to fill the gap between the increasing need of parameter selection for image processing algorithms and the lack of such a NR-IQA algorithm that makes full use of the available information.

Haoyi Liang and Daniel S. Weller are with the Charles L. Brown Department of Electrical and Computer Engineering, University of Virginia, Charlottesville, VA 22904 USA (email: hl2uc@virginia.edu, dweller@virginia.edu).

IQA algorithms are classified based on whether the reference image (the distortion-free image) is required: full-reference (FR), reduced-reference (RR) and no-reference (NR). FR-IQA [8]–[13] is a relatively well-studied area. Traditional methods like mean squared error (MSE) and signal-to-noise ratio (SNR) are used as the standard signal fidelity indices [14]. A more sophisticated FR-IQA algorithm, Structural Similarity Index Method (SSIM) [9], considers the structure information in images and performs well in different studies [14]–[17]. RR-IQA algorithms [18]–[20] require some statistical features of the reference image, such as the power spectrum, and measure the similarity of these features from the reference image and the distorted image. NR-IQA algorithms adopt two different approaches. The first kind of NR-IQA [21]–[27] has a similar approach to the RR-IQA. The difference is that rather than extracting the features from the reference images, this kind of NR-IQA extracts statistical features from a training set. The second kind of NR-IQA algorithms [7], [17] adopts a local approach to quantifying structure as a surrogate for quality. A common implementation of the second approach calculates local scores by analyzing the quality of gradient. The overall score is synthesized by taking the average of the local scores.

Among these three kinds of IQA algorithms, speed and accuracy generally decrease from FR-IQA, RR-IQA to NR-IQA progressively. Unfortunately, reference images do not exist in many cases. Noticing that in many applications, including parameter selection and comparison of different restoration algorithms, we compare a set of distorted images with the same image content, a new comparison-based IQA (C-IQA) method is proposed in this paper. The prototype of comparison-based IQA is reflected in [23]. However, the concept of comparison in [23] is just implicitly mentioned by sorting the overall image qualities of a series of distorted images. In our work, the comparison-based framework is built from low level image structures, and the final output is a graph that can illustrate the local relative quality.

After proposing the comparison-based IQA method, we demonstrate one of its applications, parameter selection. The framework of parameter trimming, first proposed in [6], is designed to boost the parameter selection by combining NR-IQA with parameter selection. In [6], parameters that do not show the potential to obtain the best result are cut during the convergence process.

The rest of the paper is organized as follows. Section II introduces and compares different NR-IQA methods. Section III elaborates on the implementation details of C-IQA. The framework of parameter trimming and the technique used

for image reconstruction are introduced in Section IV. In Section V experiments are conducted on two widely used IQA databases, LIVE [28] and CSIQ [8], to verify the accuracy of C-IQA and demonstrate the effectiveness of parameter trimming combined with C-IQA. Section VI reviews the novelty and experimental results of C-IQA and suggests extensions to comparison-based IQA.

II. EXISTING NR-IQA METHODS

Existing NR-IQA algorithms can be classified into two types [17]: global approaches and local approaches. The output of global approaches is a scalar number that indicates the overall quality of the image. The local approaches estimate the quality in each local patch, and an overall quality index is obtained by taking the average of the local quality indices.

A. Global Approach

The rationale behind global approaches [21]–[27] is that the distributions of natural scene statistics (NSS) share certain common characteristics among distortion-free images, and distortions will change these characteristics. For example, it is widely-accepted that the wavelet coefficients of a natural image can be modeled by a generalized Gaussian distribution (GGD) [29], [30].

Because the NSS are extracted from the whole image, the final output of global approaches is a scalar number that indicates the overall quality. The advantage of global NR-IQA algorithms is that most of them are not dedicated to a specific distortion since the NSS features are a high-dimensional vector designed to be sensitive to various distortions. However, because of the high dimensionality of the statistical feature space, it is difficult to individually interpret and analyze these features quantitatively, and thus feature selection is largely an empirical work. In BRISQUE [22], the authors treat this approach like a black box. Another drawback of the global approach is that computing these NSS features is usually time-consuming.

B. Local Approach

The output of the local approach [7], [17], [23] can be a graph, which illustrates the local image quality, or a scalar number by taking the average of the graph. Because in most cases the perceived distortion varies across regions in an image, an innate advantage of the local approach is that they are able to highlight the areas where distortion is most significant. At the same time, an overall quality index is easily obtained from the local quality index. Because human eyes are highly sensitive to the gradient in images, and the information in images can be well represented by their gradient [7], [9], [31], the local quality index is usually evaluated using the spatial gradient information. However, the amount of the gradient, or total variation, itself is not a stable indicator of the quality [17]. Previous works [7], [17], [32] have shown that assessing the quality of the gradient in an image can be a promising way to evaluate the image quality. Among these works, MetricQ [7] shows encouraging results choosing

denoising parameters. The underlying rationale of MetricQ is that the more concentrated the gradient direction is, the better the quality of the patch is. It is a reasonable assumption since both of the two most common distortions, noise and blurring, disperse the distributions of the gradient direction. Because C-IQA makes use of the quality index defined in MetricQ, we introduce MetricQ in detail in the next paragraphs.

The local quality index used by MetricQ is based on singular values of the local gradient matrix, which have been widely used as low level features in different image processing problems, such as tracking feature selection [33], recognition [34] and image quality assessment [17]. For each $n \times n$ local patch (w), the gradient matrix is

$$G = \begin{bmatrix} \vdots & \vdots \\ p_x(k) & p_y(k) \\ \vdots & \vdots \end{bmatrix}, \quad (1)$$

in which $p_x(k)$ and $p_y(k)$ are the gradients of the k^{th} pixel in the patch w on x and y directions. The SVD of the gradient matrix, G , is defined as

$$G = USV^T = U \begin{bmatrix} s_1 & 0 \\ 0 & s_2 \end{bmatrix} [V_1 \ V_2]^T, \quad (2)$$

where U and V are both orthonormal matrices. Vector V_1 is of size 2×1 and corresponds to the dominant direction of the local gradient; V_2 is orthogonal to V_1 and thus represents the edge direction. Singular values, s_1 and s_2 , represent the luminance variances on V_1 and V_2 respectively. Intuitively, a large s_1 and a small s_2 indicate a prominent edge in the local patch.

In MetricQ [7], two indices reflect the quality of a local patch: Image Content Index and Coherence Index. Image Content Index is defined as

$$Q = s_1 \frac{s_1 - s_2}{s_1 + s_2}, \quad (3)$$

and Coherence Index is defined as

$$R = \frac{s_1 - s_2}{s_1 + s_2}. \quad (4)$$

Q reflects the structure prominence in a local patch and R is used to determine whether a local patch is dominated by noise. The overall score of an image is calculated by

$$AQ = \frac{1}{MN} \sum_{i,j:R(i,j)>\tau} Q(i,j), \quad (5)$$

where $M \times N$ is the size of the image and τ is the threshold to decide whether a local patch is dominated by noise. $Q(i,j)$ and $R(i,j)$ are the Image Content Index and Coherence Index of the local patch centered at (i,j) in the image. A simplified interpretation of (5) is that AQ is the average structure index of local patches that have meaningful image content.

However, because the view of the local approaches is constrained by the patch size, local approaches tend to confuse the sharpness with the blocking artifacts. Fortunately, specialized IQA algorithms aimed at blocking artifacts can be used to evaluate this special distortion [26], [35].

III. COMPARISON-BASED IMAGE QUALITY ASSESSMENT

Previous works on IQA [2]–[5], [9], [12], [23], [36] show that IQA performance can be significantly improved by taking advantage of the characteristics of HVS. For example, the structural information that human eyes are highly sensitive to is made use by SSIM [9]. Traditional NR-IQA algorithms also try to exploit HVS features and make reasonable assumptions about the natural scene images, but one important aspect of HVS is ignored: comparison. In the subjective IQA experiment [8], volunteers are required to evaluate the quality of an image by comparing it with a reference image, rather than giving an absolute score for the image. Although in most image processing applications, the reference image does not exist, a set of differently degraded images are available. In these cases, extending existing state-of-the-art FR-IQA algorithms to comparison-based NR-IQA algorithms is a natural thought. However, different from FR-IQA algorithms, neither of the two input image qualities is known in the comparison-based IQA framework. As a result, in a comparison-based NR-IQA algorithm, we not only measure the difference between two input images, but also assess the quality of the difference.

A. Framework of C-IQA

As shown in Fig. 1, C-IQA has two input images, I_1 and I_2 , and the output indicates the relative quality of I_1 based on I_2 . We refer to the second image in C-IQA as the base image to distinguish it from the reference image in FR-IQA. C-IQA consists of two basic modules: Content Detection and Contribution. The third module, Texture Compensation, is optional and its description is deferred to Section III-C. In the rest of the paper, we refer to the comparison-based IQA variation composed by the two basic modules as C-IQA and the variation with three modules as CT-IQA. Content Detection determines whether the difference between two input images contains any meaningful structure, and Contribution decides which image mainly contributes to the difference. C-IQA composes these two modules by the criterion that the input image that contributes to a structured difference is better and the input image that contributes to a random difference is worse. The Texture Compensation module added in CT-IQA adjusts the distortion sensitivity difference of patches with different texture complexity [9], [37].

1) *Content Detection*: The Content Detection module is based on the Image Content Index put forward in MetricQ [7]. Different from MetricQ, this index is calculated with the difference image between two input images in C-IQA. In MetricQ, limited by the information provided by single input image, the algorithm does not know the texture complexity in the original image, and it is hard for an algorithm to tell how concentrated the gradient should be. However, by mimicking the comparative way HVS works, C-IQA removes the main image content in the images by taking the difference, and thus the Content Detection module is less influenced by the texture complexity in images.

In Alg. 1, P_1 and P_2 are two patches of size $n \times n$ from I_1 and I_2 respectively, G is the same 2-column gradient matrix defined in (1), $SVD(G)$ represents taking the SVD operation

Algorithm 1 Content Detection

```

 $D_p = P_1 - P_2$ 
 $G = [d_x(D_p) \ d_y(D_p)]$ 
 $USV^T = SVD(G)$ 
 $C_{ind} = \frac{s_1 - s_2}{s_1 + s_2}$  ▷  $s_1 > s_2$ 
if  $C_{ind} > C_{thresh}$  then
     $is\_stru = 1$  ▷ structure
else
     $is\_stru = -1$  ▷ noise
end if

```

Algorithm 2 Contribution

```

 $D_p = P_1 - P_2$ 
 $M_p = \max(\frac{mean(P_1) + mean(P_2)}{2}, \frac{1}{n \times n})$ 
 $ctri1 = cov(P_1, D_p)$ 
 $ctri2 = cov(P_2, -D_p)$ 
 $ctri = \frac{ctri1 - ctri2}{M_p}$ 

```

on G , and s_1 and s_2 are the singular values of G . C_{thresh} is a constant threshold to binarize C_{ind} . The binary output is_stru indicates whether there is a meaningful structure in the difference of local patches.

2) *Contribution*: Once the difference is classified into noise or structure, the Contribution module is designed to find out which of the two input images mainly contributes to the difference image. In our implementation, the luminance-normalized covariance between the input image and the difference image is used to measure the contribution.

In Alg. 2, $mean(P_i)$ calculates the average of the local patch, and $cov(x_1, x_2)$ calculates the covariance between two input patches,

$$cov(x_1, x_2) = \frac{(x_1 - mean(x_1))^T (x_2 - mean(x_2))}{n^2 - 1},$$

x_1 and x_2 are vectorized patches of size $n^2 \times 1$.

The comparative quality index for each local patch is calculated by

$$C_Q = is_stru \cdot ctri.$$

The overall comparative quality of I_1 based on I_2 is

$$CIQA(I_1, I_2) = \frac{1}{M \times N} \sum_{i,j=(n/2):(M-n/2)} C_Q(i, j),$$

where $C_Q(i, j)$ is the local comparative quality index centered at (i, j) in the image, $n \times n$ is the size of the local patch and $M \times N$ is the size of the image. Pixels that are on the margin of the image do not have C_Q and thus are not included for the overall quality. A positive $CIQA(I_1, I_2)$ means I_1 is better than I_2 , and the absolute value quantifies the quality difference. Due to the anti-symmetric design of the algorithm, $CIQA(I_1, I_2) = -CIQA(I_2, I_1)$.

B. Justification of C-IQA

Inspired Li's work [38] which claims that an IQA model should be based on three quantities: edge sharpness, random

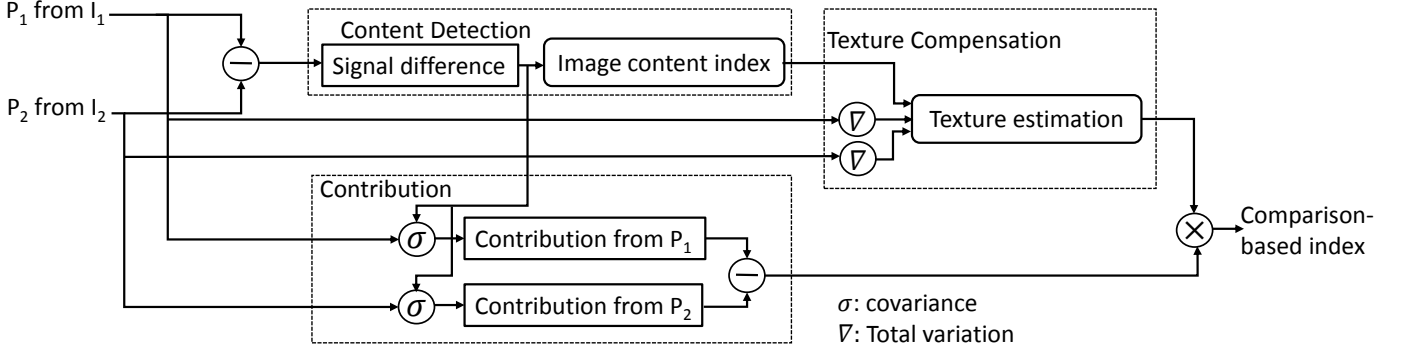


Fig. 1: Flow Chart of Comparison-based IQA: P_1 and P_2 are local patches from input images, I_1 and I_2 , at the same location respectively. The Content Detection module determines whether there is a meaningful structure in the difference patch; the Contribution module calculates which patch mainly contributes to the difference patch; the Texture Compensation module compensates the distortion sensitivity difference of patches with various texture complexities. The output, comparison-based index, indicates the relative quality of P_1 based on P_2 .

noise level and structure noise, we classify the distortions by residual images, the difference between a distorted image and the original image. In our new classification, distortions can be categorized into two types: introducing a random residual image, or introducing a structured residual image. In most cases, random residual images correspond to noise-like distortions and structured residual images correspond to blurring-like distortions. In this part, we prove how C-IQA works under these two distortions.

Assume I_{true} is the original image and I_1, I_2 are two distorted images. The residual images are calculated by,

$$e_i = I_i - I_{true}, \quad i = 1, 2.$$

Similarly, for each patch we have

$$e_{Pi} = P_i - P_{true}, \quad i = 1, 2.$$

a) *Random residual image*: Residual images behave like noise in this case. If we assume I_1 is more severely distorted than I_2 , then we have $E[\|e_{P1}\|_2^2] > E[\|e_{P2}\|_2^2]$. The expectation of the local comparative quality index is

$$\begin{aligned} E[C_Q] &= E[ctri \cdot is_stru] \\ &= E[(ctri1 - ctri2) \cdot is_stru] \\ &= E[cov(P_1, P_1 - P_2) - cov(P_2, P_2 - P_1)] \\ &\quad \cdot E[is_stru] \\ &= -E[cov(P_{true} + e_{P1}, e_{P1} - e_{P2}) \\ &\quad - cov(P_{true} + e_{P2}, e_{P2} - e_{P1})] \\ &= -E[2 \cdot cov(P_{true}, e_{P1} - e_{P2}) \\ &\quad + cov(e_{P1}, e_{P1}) - cov(e_{P2}, e_{P2})] \\ &= -E[cov(e_{P1}, e_{P1})] + E[cov(e_{P2}, e_{P2})] \\ &< 0. \end{aligned}$$

The three most important properties in the derivation are the irrelevance between P_{true} and e_{Pi} , the randomness of e_{Pi} , and independence of is_stru and $ctri1, ctri2$. The result $E[C_Q] < 0$ agrees with our assumption that I_1 is more severely distorted than I_2 and when I_2 is more severely distorted, the same proof shows $E[C_Q] > 0$.

b) *Structured residual image*: If the residual images show structured information, the most probable reason is that the image is distorted by a blurring-like distortion. Because the blurring filter acts as a low-pass filter, the residual images show a structure that is inversely related to the original image [39] to smoothen the high contrast on the edges.

Without loss of generality, we assume more blurring happens in I_1 than I_2 , which means $E[\|e_{P1}\|] > E[\|e_{P2}\|]$. The expectation of the local comparative quality index is

$$\begin{aligned} E[C_Q] &= E[ctri \cdot is_stru] \\ &= E[(ctri1 - ctri2) \cdot is_stru] \\ &= E[cov(P_1, P_1 - P_2) - cov(P_2, P_2 - P_1)] \\ &= E[cov(P_{true} + e_{P1}, e_{P1} - e_{P2}) \\ &\quad - cov(P_{true} + e_{P2}, e_{P2} - e_{P1})] \\ &= E[cov(2 \cdot P_{true}, e_{P1} - e_{P2}) \\ &\quad + cov(e_{P1} + e_{P2}, e_{P1} - e_{P2})] \\ &= E[cov(2 \cdot P_{true} + e_{P1} + e_{P2}, e_{P1} - e_{P2})] \\ &< 0. \end{aligned}$$

The most important step in this derivation is the last step. Since $E[\|e_{P1}\|] > E[\|e_{P2}\|]$, $e_{P1} - e_{P2}$ also demonstrates a structure that is inversely related to the original image as e_{Pi} . As long as the distortion is not severe enough to remove the structure in the original image, $2 \cdot P_{true} + e_{P1} + e_{P2} = P_1 + P_2$ is positively related to the original image. As a result, $E[cov(2 \cdot P_{true} + e_{P1} + e_{P2}, e_{P1} - e_{P2})] < 0$, which agrees with our assumption that I_1 is more severely distorted than I_2 . Following the same steps, we can show $E[C_Q] > 0$ if I_2 is more severe distorted than I_1 .

C. Texture Compensation

We have proven that only with Content Detection and Contribution, the C-IQA can give correct results if both of the two input images are distorted by one distortion, either noise-like distortion or blurring-like distortion. However, another important property of HVS is missed in C-IQA: the response

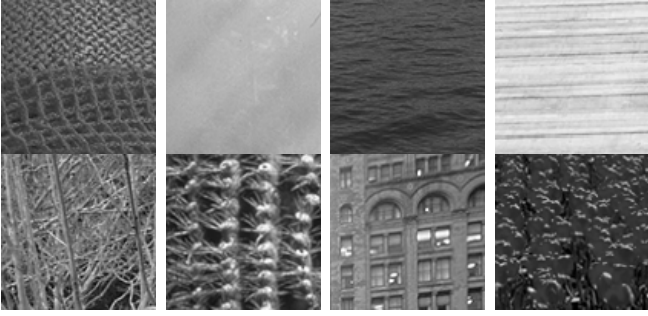


Fig. 2: Patch samples are selected from LIVE [28] and CSIQ [8] to verify the texture compensation in C-IQA.

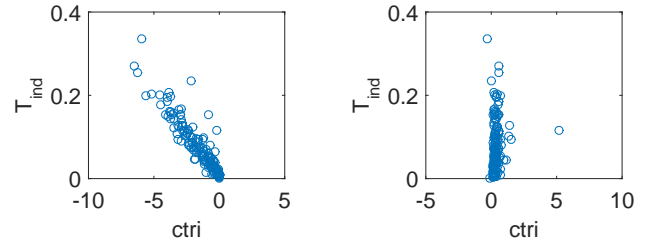
of HVS to the same distortion is texture-dependent. One example of this HVS property is that after being distorted by the same amount of Gaussian noise, the distortion in the image with simpler texture is more obvious. In this part, we first investigate such texture-based response of C-IQA and then design a compensation algorithm to adjust the sensitivity of C-IQA to different textures. We refer to the improved C-IQA as CT-IQA.

In C-IQA, Content Detection is a qualitative module that detects the meaningful structure and the Contribution module quantifies the relative quality. Therefore, the Contribution module may implicitly include compensation. We design an experiment to explore the relation between the texture complexity and the output of Contribution, $ctri$. In this experiment, 140 patches of size 101×101 with homogeneous texture are selected from LIVE [28] and CSIQ [8], and six samples of these patches are shown in Fig. 2. As the representatives of blurring-like and noise-like distortions, bilateral filter and Gaussian noise with the same parameters are applied to each patch. According to the Weber-Fechner law [40], we use luminance-normalized total variation as the perceived texture complexity, $T_{ind} = \frac{TV(P)}{mean(P)}$, where $TV(P)$ is the total variation in the original patch and $mean(P)$ is the average of the original patch. The relation between T_{ind} and $ctri$ are plotted in Fig. 3, in which each circle represents a patch. From Fig. 3, it is clear that $ctri$ is almost linear related to texture complexity, T_{ind} , when blurring happens. On the contrary, T_{ind} shows no relation with $ctri$ when the distortion is noise. The reason for this is that blurring is a highly image-dependent distortion, and the residual image is more prominent at areas where total variation is high. After figuring out the blurring sensitivity compensation mechanism in C-IQA, we need to design an algorithm to compensate the sensitivity difference to noise.

Because noise-like distortion tends to increase the total variation while blurring-like distortion tends to decrease the total variation, Alg. 3 uses the output of Content Detection to synthesize $T1_{ind}$ and $T2_{ind}$ into T_{ind} . After texture complexity estimation, we transfer T_{ind} to the smoothness index, S_{ind} , and compensate the sensitivity to noise.

In CT-IQA, the comparative quality index for each local patch is

$$CT_Q = is_stru \cdot ctri \cdot weight.$$



(a) Blurring ($\rho = -0.92$) (b) Noise ($\rho = 0.10$)

Fig. 3: Relations between $ctri$ and T_{ind} . Each circle in the figure represents a sample patch. All the sample patches are degraded by the same amount of distortion for blurring and noise.

Algorithm 3 Texture Compensation

```

 $T1_{ind} = \frac{TV(P_1)}{mean(P_1)}$ 
 $T2_{ind} = \frac{TV(P_2)}{mean(P_2)}$ 
if  $is\_stru = 1$  then
     $T_{ind} = \max\{T1_{ind}, T2_{ind}\};$ 
else
     $T_{ind} = \min\{T1_{ind}, T2_{ind}\};$ 
end if
 $S_{ind} = \log(1 + \frac{1}{C_1 \times T_{ind}})$ 
if  $is\_stru = 1$  then
     $weight = 1$ 
else
     $weight = -S_{ind}$ 
end if

```

The overall comparative quality of I_1 based on I_2 is calculated by taking the average of local comparative quality index as C-IQA does.

D. Comparison between CT-IQA and SSIM

SSIM consists of three components: structure (loss of correlation), luminance (mean distortion) and contrast (variance distortion). In CT-IQA, the outputs of Content Detection and Texture Compensation provide a “reference image” (the difference image) and the quality of the “reference image”. The luminance and the contrast of an input image together determine the contribution of the input image to the “reference image”. Therefore, Content Detection and Texture Compensation of CT-IQA together play the role of the structure part in SSIM. The difference is that without knowing which image has the better quality, CT-IQA has to analyze the quality of the structure in the “reference image”, rather than only measuring the structure distance as SSIM does. The Contribution module in CT-IQA is similar to the functions of luminance and contrast parts together in SSIM.

IV. PARAMETER SELECTION

As the motivation of C-IQA mentioned in the introduction, most image processing algorithms contain user-defined parameters (these image processing algorithms are referred as “target algorithms” in the following to differ from IQA algorithms).

Parameter selection [6], [7], [41]–[47] is of importance to these target algorithms. By parameter selection, some of these target algorithms [45], [46] achieve a faster convergence rate; some [43], [44] obtain a better restored image.

A traditional approach to parameter selection [41]–[44] is selecting the parameters after the convergence of all the target algorithm instances with a perceptual quality monitor, usually a NR-IQA algorithm. However, since either the target algorithms converge quickly [7], [44] or the NR-IQA algorithm is time-consuming [43], computational efficiency is not considered in previous works. For instance, the denoising parameter selection in [7] involves experiments with 30 parameter candidates and 20 iterations/candidate. In situations where target algorithms converge slowly or the set of parameter candidates is large, assessing image qualities and selecting the best parameter after all the algorithm instances converge would be too time-consuming to be practical. Instead of placing the quality monitor at the output end, a novel parameter trimming framework proposed in [6] integrates the quality monitor into the target algorithms. By doing so, parameters that do not have the potential to achieve good results are trimmed before convergence. In this section, we use image reconstruction as the application to illustrate the parameter trimming framework because a regularized iterative algorithm is usually adopted to obtain superior reconstructed results.

A. Image Reconstruction

Total variation (TV) reconstruction [48] is aimed at minimizing the cost function,

$$E_\beta(x) = \beta \|Dx\|_1 + \frac{1}{2} \|Sx - y\|_2^2, \quad (6)$$

where x is the reconstructed image, y is the observed incomplete data set, S is the system matrix, D represents the difference matrix, and the TV regularizer $\|Dx\|_1$ combines gradients on two directions isotropically. In our implementation, $S = R\mathcal{F}$, where R represents the subsampling matrix and \mathcal{F} represents the Fourier transform matrix. The regularization parameter β controls the sharpness of the reconstructed result. Large β will oversmooth the reconstructed image, while small β will leave residual noise. A proper β is crucial to the performance of TV reconstruction. Split Bregman iteration [49] is used to solve (6). By making the replacement $d \leftarrow Dx$ and introducing the dual variable b , the split formulation of (6) becomes:

$$\min_{x,d} \beta \|d\|_1 + \frac{1}{2} \|Sy - y\|_2^2 + \frac{\mu}{2} \|d - Dx - b\|_2^2, \quad (7)$$

s.t. $d = Dx$.

The Split Bregman iteration solution to (7) is Alg. 4. In Alg. 4 we use the notation $K = (R^T R - \mu \mathcal{F} D^T D \mathcal{F}^{-1})$, $L_k = (\mathcal{F}^T R^T y + \mu D^T (d^k - b^k))$ and $s^k = \sqrt{|Dx^k + b^k|^2}$. μ is set as 0.01β to ensure a fast convergence rate.

To illustrate the necessity of parameter selection of TV reconstruction, the Brain image [50] is reconstructed with 30 values of β . These candidate values of β are uniformly sampled from 1.22×10^{-6} to 10 in logarithmic scale and three of the reconstructed results are shown in Fig. 4. The image

Algorithm 4 Split Bregman

Initialize: $x^0 = 0, d^0 = b^0 = 0$

while stop criterion is not satisfied **do**

$$x^{k+1} = \mathcal{F}^{-1} K^{-1} L_k$$

$$d_{k+1} = \max\left(s^k - \frac{1}{\mu}, 0\right) \frac{Dx^k + b^k}{s^k}$$

$$b^{k+1} = b^k + (Dx^k - d^{k+1})$$

end while

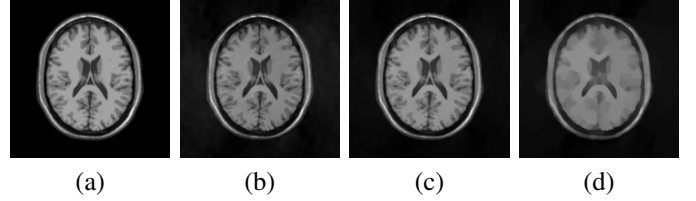


Fig. 4: (a): original Brain image [50]; (b): reconstructed result with $\beta = 1.22 \times 10^{-6}$; (c): reconstruction result with $\beta = 4.46 \times 10^{-1}$; (d): reconstructed result with $\beta = 10$.

quality indices during the convergence process are plotted in Fig. 5(a), and each line corresponds to one parameter candidate. The final reconstructed image qualities are plotted in Fig. 5(b).

B. Parameter trimming

In [6], we first proposed a parameter trimming framework that combines the quality index with target algorithms to carry out the parameter selection before convergence. Assume I_m^i is the reconstructed result of the m^{th} parameter candidate at the i^{th} iteration. The trimming decision is made based on three indices, s_m^i , g_m^i and p_m^i , which are the reconstructed quality, the quality increasing gradient and the prediction of the quality of I_m^i respectively. Because the image quality index we use here is a comparison-based index, the definitions of these three indices are modified to fit CT-IQA into the parameter trimming framework in [6]. Denoting the best reconstructed result at the i^{th} iteration is $best_i$, it satisfies $CTIQA(I_{best_i}^i, I_{best_i-1}^i) \geq 0$ and $CTIQA(I_{best_i}^i, I_{best_i+1}^i) \geq 0$. The three indices used for parameter trimming, s_m^i , g_m^i and p_m^i , are defined as,

$$s_m^i = CTIQA(I_m^i, I_{best_i}^i),$$

$$g_m^i = CTIQA(I_m^i, I_{best_i-1}^{i-1}) - CTIQA(I_m^{i-1}, I_{best_i-1}^{i-1}),$$

$$p_m^i = s_m^i + pre_{len} \cdot g_m^i.$$

We set $pre_{len} = 4$ in all the experiments. More examples of the reconstruction process and the changing of these three indices during the trimming process are shown in Section V.

V. EXPERIMENTS

We first introduce two key properties (consistency and minimum resolution) of C-IQA/CT-IQA in Section V-A. In the next two parts, more comprehensive experiments on two

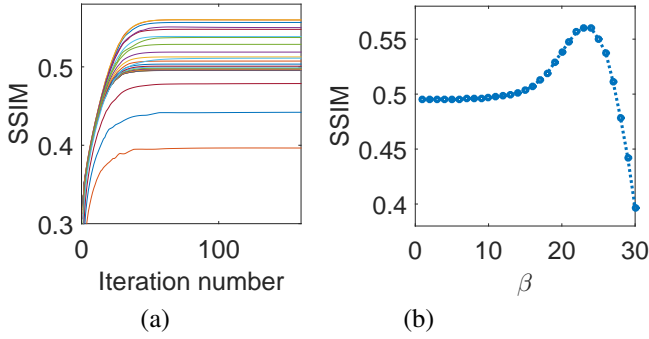


Fig. 5: (a): Each line corresponds to an algorithm instance with a parameter candidate. (b): Reconstructed result qualities of different parameter candidates after 160 iterations.

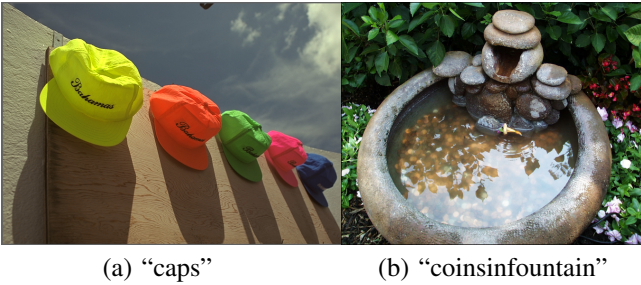


Fig. 6: Images from LIVE [28] used for case study in Section V-A

databases are conducted to verify the effectiveness of C-IQA/CT-IQA and their applications to parameter selection.

The other NR-IQA algorithms that we use to compare C-IQA/CT-IQA with are DIIVINE (DII) [21], BRISQUE (BRI) [22], MetricQ (MQ) [7] and Anisotropy (Ani) [23]. A widely accepted FR-IQA algorithm, SSIM [9], is used as the ground truth to evaluate the performance of different NR-IQA algorithms. Two IQA databases used in the experiments are LIVE [28] and CISQ [8]. Parameters in C-IQA/CT-IQA are set as $C_{thresh} = 0.12$, $C_1 = 4.6$ and the size of local patch is 9×9 .

A. Case study to explore two key properties of C-IQA/CT-IQA

Since the comparison-based IQA is a brand-new approach, some new properties arise. In this section, we illustrate these properties and corresponding solutions based on two images from LIVE [28] as shown in Fig. 6.

1) *Consistency on single kind of distortion*: Consistency on a single kind of distortion is one of the basic requirements of an IQA algorithm. Because distortions can be generally classified into two categories [51], noise and blur, we check the consistency of different NR-IQA algorithms on Gaussian noise and blurring with the Gaussian kernel respectively.

For each distortion, a series of increasingly distorted images, whose SSIM indices uniformly range from 0.85 to 1, are evaluated by different NR-IQA algorithms. Since we are interested in the trend of each IQA algorithm, scores obtained from different IQA algorithms are normalized between [0, 1] and the original images are used as the base images for C-IQA/CT-IQA. It is clear from Fig. 7 that all of NR-IQA

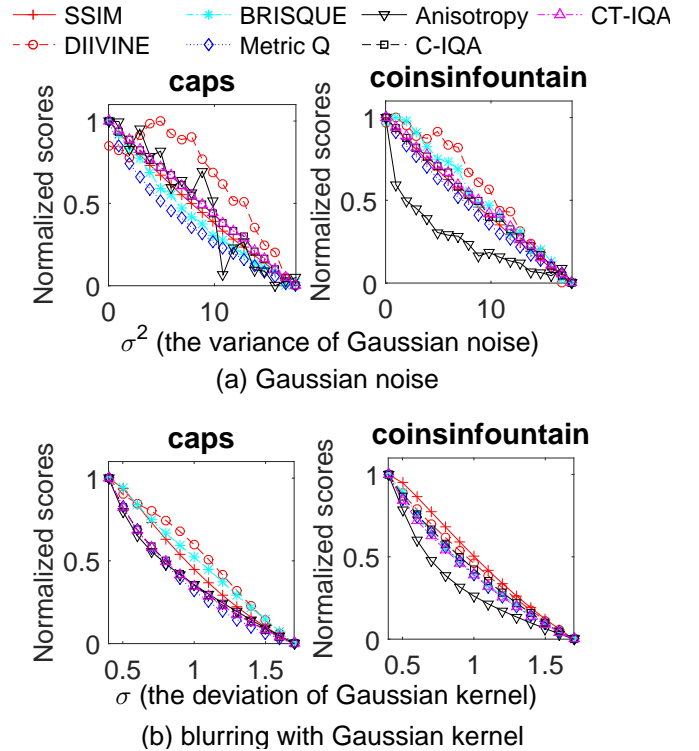


Fig. 7: Consistency of different IQA algorithms on noise and blurring. The scores of Anisotropy and DIIVINE are inconsistent on Gaussian noise.

algorithms produce consistent results for blurring, but in the noise case, DIIVINE and Anisotropy are inconsistent.

2) *Minimum resolution*: Similar to HVS, IQA algorithms are not able to make a convincing quality comparison between images whose difference is sufficiently small. In this part, we define the minimum mean squared difference (MSD) between two images required to make a convincing quality comparison as the minimum resolution. It is worth noticing that minimum resolutions vary over different distortions and different IQA algorithms.

For the traditional single-image-input NR-IQA algorithms, minimum resolutions can be regarded as the minimum MSD required to ensure consistency on a series of increasingly distorted images. The unwanted fluctuations of DIIVINE and Anisotropy in Fig. 7(a) indicate that the MSD between the adjacent images is less than their minimum resolutions of Gaussian noise.

However, under the comparison-based framework, a distorted image has different scores compared with different base images. We cannot refer to the consistency to define the minimum resolution for a comparison-based IQA algorithm. The minimum resolution for comparison-based IQA is defined as the minimum MSD required to preserve transitivity among a series of distorted images. We conduct an experiment on the images in Fig. 6 to demonstrate the transitivity. Assume I_{org} is the original image, and I_1 is created by adding Gaussian noise to I_{org} . A series of gradually filtered images, (I_1, I_2, \dots, I_N) , are denoised by bilateral filters $BF_{(r,d)}$, where r and d are the variances of Gaussian range kernel for smoothing differences

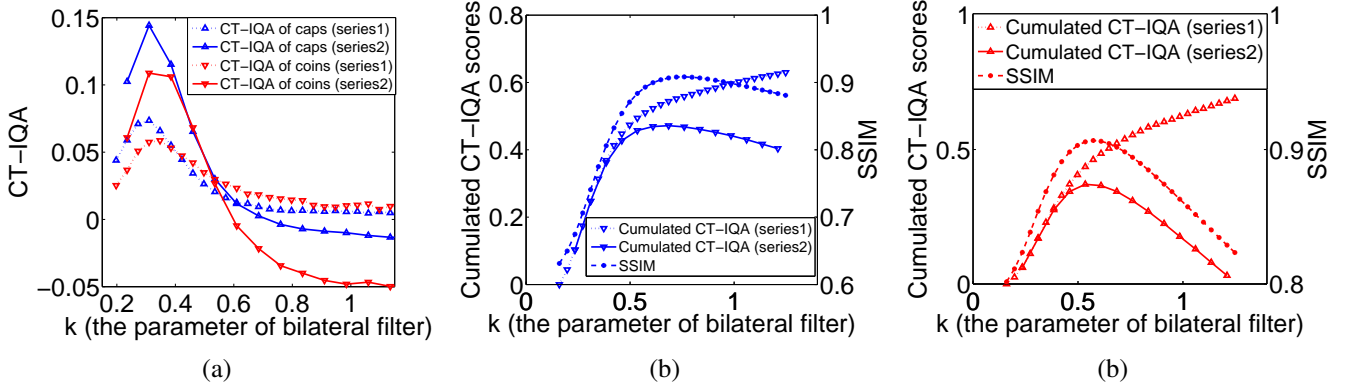


Fig. 8: Minimum resolution of Comparison-based IQA algorithm: (a) CT-IQA scores of denoised images compared with their previous images (*series1*) and the one before previous images (*series2*); (b) Accumulated CT-IQA scores in (a) and SSIM scores of “caps”; (c) Accumulated CT-IQA scores in (a) and SSIM scores of “coinsinfountain”

in intensities and Gaussian spatial kernel for smoothing differences in coordinates. For simplicity, we reduce the parameters of bilateral filters to one by fixing the ratio between r and d , $BF_k = BF_{(0.1k, 3k)}$. In Fig. 8(a), we show the CT-IQA scores of each image compared with its previous one in the denoised sequence (*series1*) and the CT-IQA scores compared with the one before its previous one (*series2*). We can see that CT-IQA scores in *series1* are always positive, but pass 0 in *series2*, which means the denoised image qualities are monotonically increasing in *series1*, but reach a peak in *series2*. In Fig. 8(b) and Fig. 8(c), we plot the cumulated CT-IQA scores in *series1* and *series2*. It is clear that CT-IQA fails to characterize the trend of image quality in *series1*, but successfully reflects the peak in *series2*. In this example, the MSD between adjacent images in *series1* is below the minimum resolution of the bilateral filter, but the MSD between adjacent images in *series2* is above the minimum resolution of the bilateral filter.

There are two ways to avoid the unwanted result of operating below minimum resolution. First, increase the difference between adjacent images by increasing the parameter steps. Second, avoid comparing the adjacent images in a series of increasingly distorted images. The Key Image algorithm introduced in the next part is an implementation of the second way.

B. Experiment verification on databases

In this part, we evaluate the performance of different NR-IQA algorithms by comparing their balance abilities between noise and blurring on two databases.

1) *Balance ability among different distortions*: In this experiment, four distortions are applied to each original image and four series of increasingly distorted images are created: independent and identically distributed Gaussian noise (IID-GN), Zero-mean Gaussian noise with an intensity-dependent variance (ID-GN), blurring with Gaussian kernel (GB) and blurring with bilateral filter (BB). We reduce the parameters of the bilateral filter to one parameter the same way as we did in Section V-A. For each image under each kind of distortion,

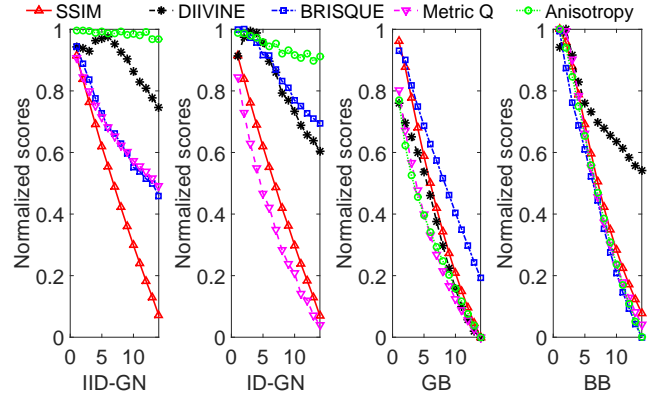


Fig. 9: IQAs scores of 60 degraded “caps” by four distortions

we first search the distortion parameter to ensure the SSIM index of the distorted image is between 0.85 ± 0.01 , and then uniformly sample the other 14 parameters between 0 and the searched distortion parameter. In Fig. 9, we show the IQA scores of 60 distorted “caps” by different IQA algorithms. All the scores are also normalized to $[0, 1]$ for each IQA algorithm.

Since it is justified for each IQA algorithm to have its own sensitivity properties at different distortion levels, we evaluate the balance ability among different distortions of each NR-IQA algorithm at 14 distortion levels. Eight distorted images with adjacent distortion parameters of four distortions are combined into an image set. The average SSIM index of all the eight images is the distortion level of this set. Therefore, we have 14 sets of distorted images and rank the eight distorted images in each set according to different IQA algorithms. The weighted inversion numbers [52] between the ranking results by NR-IQA algorithms and by SSIM are used to evaluate the performance of different NR-IQA algorithms. Assume (I_1, \dots, I_N) is the ranking sequence according to a NR-IQA algorithm from low quality to high quality, the weighted inversion number in our experiment is defined as

$$WInv_{num} = \sum_{i=1:N} \sum_{j=i+1:N} \max(0, SSIM(I_i) - SSIM(I_j)).$$

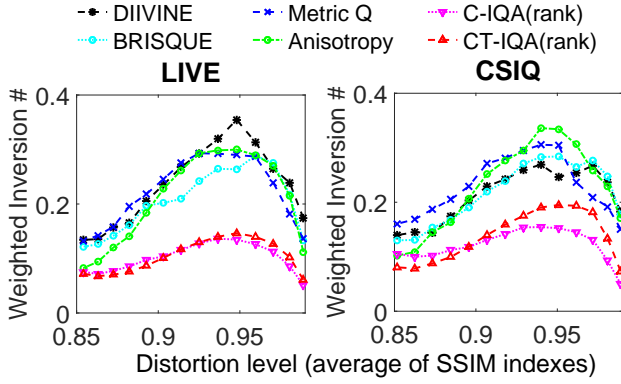


Fig. 10: Weighted inversion numbers of different NR-IQA methods at 14 distortion levels

Since C-IQA/CT-IQA are rank-based algorithms, distorted images in one set are sorted by the bubble sort algorithm. The bubble sort algorithm is the same as the traditional one, except that we use C-IQA/CT-IQA to compare each adjacent pair of images in the ranking sequence. In our experiment, the final ranking results are not sensitive to the initial ranking and we start the bubble sort from a random rank. Fig. 10 shows weighted inversion numbers at 14 distortion levels on two databases.

In Table I, we provide the average weighted inversion numbers over 14 distortion levels of different NR-IQA algorithms. It is clear C-IQA and CT-IQA are two of the best NR-IQA algorithms.

2) *Balance ability for bilateral filter*: A series of increasingly denoised images by bilateral filtering, I_1, I_2, \dots, I_{30} , is created for each image the same as the previous part. The SSIM index of the most oversmoothed image I_{30} is between 0.85 ± 0.01 . Because the MSD between the adjacent images are below minimum resolution, Alg. 5 is adopted to select the best result. Key images are a set of images among which the MSD is greater than the minimum resolution. Alg. 5 first separates the 30 increasingly distorted images into a few parts by key images. Images in the two parts next to the best key image are evaluated based on the two key images on the ends. By doing so, we avoid comparing the adjacent images directly. We set $K_{thresh} = 3.0$ in this experiment.

The SSIM index difference between the best images chosen by a NR-IQA method and the one chosen by SSIM is used to evaluate NR-IQA methods. There are 59 original images in the two databases and 1770 distorted images in our experiment. From Fig. 11, we can see that MetricQ and CT-IQA are two of the best NR-IQA algorithms. Table II provides more quantitative evaluations of different NR-IQA algorithms.

In order to have a better understanding of Comparison-based IQA, we show two outliers of C-IQA/CT-IQA in Fig. 12. Without the knowledge of the contents in the scenes, fine textures are regarded as noise in these two images, and both C-IQA/CT-IQA choose oversmoothed images as the best denoised results.

3) *Balance ability for TV reconstruction*: The algorithm used for image reconstruction is introduced in Section IV-A.

Algorithm 5 Key Image

Key Images Selection;

```

key_img = [1]
key_num = 1
for i = 1 : N do
    if  $MSE(I_i, I_{pre\_key(key\_num)}) > K_{thresh}$  then
        key_img = [key_img, i]
        key_num = key_num + 1
    end if
end for

```

Key Images Comparison;

```

for i = 2 : (key_num - 1) do
    if  $CQ(I_{key\_img(i)}, I_{key\_img(i-1)}) > 0$  and
        $CQ(I_{key\_img(i)}, I_{key\_img(i+1)}) > 0$  then
        best_key = i
        break;
    end if
end for

```

Best Image Selection;

```

start_num = key_img(best_key - 1)
end_num = key_img(best_key + 1)
for i = start_num : end_num do
    score_start(i) =  $CQ(I(i), I(start\_num))$ 
    score_end(i) =  $CQ(I(i), I(end\_num))$ 
end for
best_img = max(score_start + score_end)

```

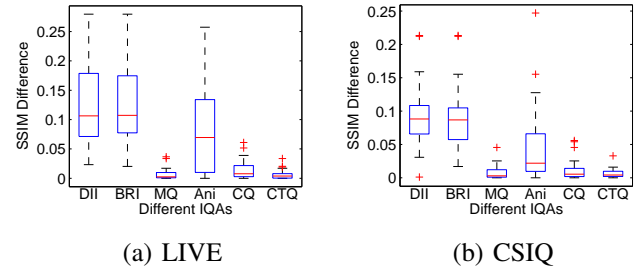


Fig. 11: The SSIM differences between the best images chosen by IQA method and by SSIM from denoised images

In the experiment, 70% Fourier transform data are used to reconstruct the image and in order to be more realistic, Fourier transform data are distorted by Gaussian noise. The SNR is kept at 20 dB in all reconstruction experiments. All 30 regularization parameter candidates are uniformly selected between $[10^{-5}, 10^{-1}]$ in logarithmic scale. Because in this experiment, the MSD between adjacent images is above the minimum resolution of C-IQA/CT-IQA, we choose the best image simply by comparing the adjacent images.

The SSIM difference of each IQA algorithm is plotted in Fig. 13. C-IQA and CT-IQA are the two best IQA algorithms. In Table III, we provide quantitative evaluation of different NR-IQA algorithms. The two outliers in TV reconstruction are the same images as shown in Fig. 12.

TABLE I: Average weighted inversion numbers of different NR-IQA algorithms

	DIIVINE	BRISQUE	MetricQ	Anisotropy	C-IQA (ranking)	CT-IQA (ranking)
LIVE	0.2328	0.2032	0.2205	0.2064	0.1001	0.1026
CSIQ	0.2137	0.2168	0.2283	0.2274	0.1207	0.1362

TABLE II: Balancing abilities of blurring and noise on a series of denoised images of different IQAs

		DIIVINE	BRISQUE	MetricQ	Anisotropy	C-IQA	C-T-IQA
LIVE	median of all SSIM differences	1.06×10^{-1}	1.07×10^{-1}	2.36×10^{-3}	6.95×10^{-2}	1.43×10^{-2}	3.80×10^{-3}
	average of all SSIM differences	1.22×10^{-1}	1.25×10^{-1}	6.73×10^{-3}	8.23×10^{-2}	1.43×10^{-2}	6.05×10^{-3}
	average of non-outliers	1.22×10^{-1}	1.25×10^{-1}	5.67×10^{-3}	8.23×10^{-2}	1.12×10^{-2}	3.93×10^{-3}
CSIQ	median of all SSIM differences	8.81×10^{-2}	8.68×10^{-2}	2.83×10^{-3}	2.18×10^{-2}	5.28×10^{-3}	4.05×10^{-3}
	average of all SSIM differences	9.11×10^{-2}	8.95×10^{-2}	7.65×10^{-3}	4.30×10^{-2}	1.09×10^{-2}	6.24×10^{-3}
	average of non-outliers	8.54×10^{-2}	8.06×10^{-2}	6.34×10^{-3}	3.17×10^{-2}	6.36×10^{-3}	5.32×10^{-3}

TABLE III: Balancing abilities of blurring and noise on a series of reconstructed images of different IQAs

		DIIVINE	BRISQUE	MetricQ	Anisotropy	C-IQA	C-T-IQA
LIVE	median of all SSIM differences	1.67×10^{-1}	1.33×10^{-1}	2.42×10^{-2}	8.88×10^{-2}	2.97×10^{-3}	0
	average of all SSIM difference	1.85×10^{-1}	1.33×10^{-1}	5.07×10^{-2}	1.09×10^{-1}	9.92×10^{-3}	7.77×10^{-3}
	average of non-outliers	1.74×10^{-1}	1.33×10^{-1}	5.07×10^{-2}	1.09×10^{-1}	7.02×10^{-3}	2.07×10^{-3}
CSIQ	median of all SSIM difference	1.24×10^{-1}	1.05×10^{-1}	2.44×10^{-2}	3.66×10^{-2}	1.73×10^{-3}	1.73×10^{-3}
	average of all SSIM difference	1.43×10^{-1}	1.23×10^{-1}	4.25×10^{-2}	4.30×10^{-2}	1.12×10^{-2}	1.12×10^{-2}
	average of non-outliers	1.31×10^{-1}	1.23×10^{-1}	2.19×10^{-2}	3.81×10^{-2}	6.02×10^{-3}	5.38×10^{-3}

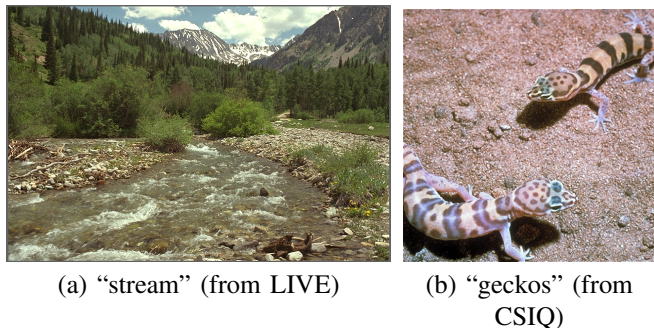


Fig. 12: Outliers of parameter selection

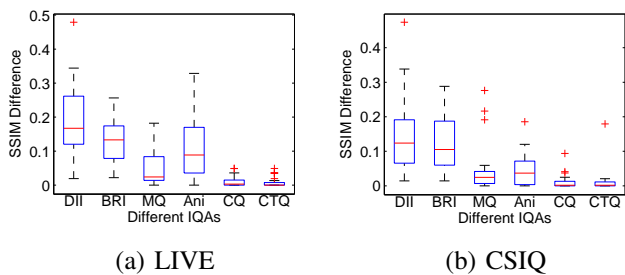


Fig. 13: The SSIM differences between the best images chosen by NR-IQA method and the by SSIM from reconstructed images

C. Application in iterative framework

In this section, we combine CT-IQA with the parameter trimming framework and show that considerable computation can be saved while preserving the accuracy of parameter selection.

1) *1-D parameter trimming*: In this part, all the parameter settings are the same as the settings in Section V-B3. On LIVE [28], all the parameters selected with parameter trimming are the same as the parameters selected after convergence; on

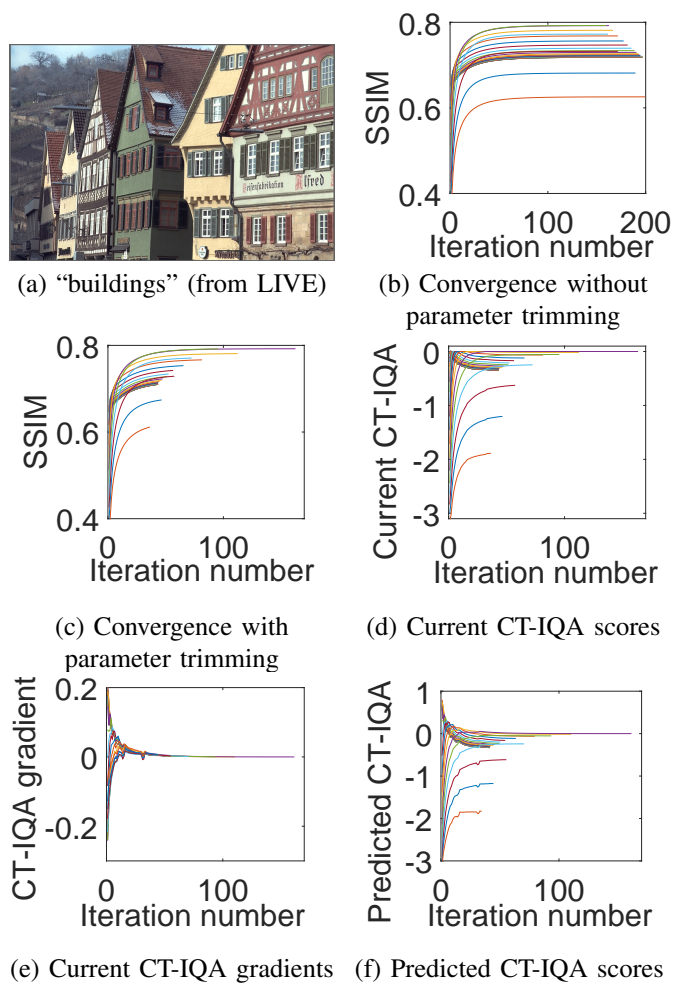


Fig. 14: Comparison between convergence with and without 1-D parameter trimming on “buildings”

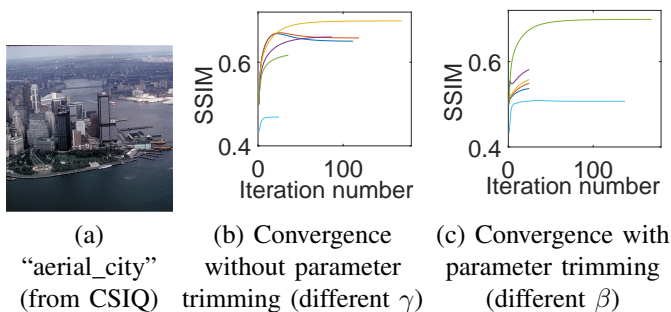


Fig. 15: Comparison between convergence with and without 2-D parameter trimming on “aerial city”

TABLE IV: Computation saved by parameter trimming

	Ave # of iteration without parameter trimming	Ave # of iteration with parameter trimming	saved computation (%)
LIVE	4651.9	847.7	81.78
CSIQ	4565.6	941.1	79.39

CSIQ [8], only one of the best parameter selected by parameter trimming is different from the one selected after convergence. Fig. 14(a) is one example image in parameter trimming. In Fig. 14(b) and Fig. 14(c), we show the effectiveness of parameter trimming with SSIM as the quality index (SSIM is only used to demonstrated the trimming process here); Fig. 14(d) -Fig. 14(f) show the changes of three CT-IQA related indices that we actually use to make the trimming decision. From Fig. 14, we can see that the trimming decision achieves the goal of terminating iteration of parameters that is far from the best choice and thus saving computation.

In Table IV, we provide the average numbers of iterations with and without parameter trimming per image on two databases.

2) *2-D parameters trimming*: We include two regularizers, TV and Haar wavelet, for the reconstruction algorithm in this part. Two regularization parameters, β and γ , are for TV and Haar wavelet respectively and both have six parameter candidates. Regularization parameters, β and γ , are uniformly sampled between $[10^{-5}, 10^{-1}]$ and $[10^{-8}, 10^{-1}]$ in logarithmic scale. One image from CSIQ [8] is tested for 2-D parameter trimming and the best set of parameters is correctly selected by parameter trimming. In Fig. 15, parameter trimming is illustrated by changing one parameter while fixing the other parameter as the best choice.

VI. CONCLUSION

In this paper, we focused on the NR-IQA method and discussed the advantages and drawbacks of two different approaches to the NR-IQA problem, global and local approaches. Inspired by some key concepts put forward in the previous works [7], [23], for the first time we designed a comparison-based IQA method and analyzed important properties unique to comparison-based IQA, such as minimum resolution. The novel C-IQA/CT-IQA method includes three primary modules, Content Detection, Contribution and Texture Compensation.

At last, the comparison-based IQA compares favorably with other NR-IQA algorithms on two widely used databases [8], [28].

In the experiment (Section V), we showed that when fine texture with small granularity appears in the image, C-IQA/CT-IQA tends to select the suboptimal result. Integrating the global texture information with local gradient-based structure information is a possible solution to improve the robustness of comparison-based IQA and other NR-IQA algorithms.

We take C-IQA/CT-IQA as a specific implementation of the comparison-based IQA method. By exploiting the extra available information in many image quality assessment applications, other comparison-based IQA methods can be designed for different application scenarios.

ACKNOWLEDGMENT

The authors would like to thank Xiang Zhu for providing the MetricQ [7] code and Anush Krishna Moorthy for explaining the usage of DIIVINE [21] code.

REFERENCES

- [1] E. P. Simoncelli and B. A. Olshausen, “Natural image statistics and neural representation,” *Annual Review of Neuroscience*, pp. 1193–1216, 2001.
- [2] P. C. Teo and D. J. Heeger, “Perceptual image distortion,” in *Proc. SPIE*, 1994, pp. 127–141.
- [3] J. Lubin, “A human vision system model for objective picture quality measurements,” in *Broadcasting Convention*, 1997, pp. 498–503.
- [4] F. XJ. Lukas and Z. L. Budrikis, “Picture quality prediction based on a visual model,” *IEEE Trans. Communications*, vol. 30, no. 7, pp. 1679–1692, Jul. 1982.
- [5] S.J.P. Westen, R.L. Lagendijk, and J. Biemond, “Perceptual image quality based on a multiple channel HVS model,” in *Proc. Int. Conf. Acoustics, Speech, Signal Processing*, 1995, vol. 4, pp. 2351–2354.
- [6] H. Liang and D. S. Weller, “Regularization parameter trimming for iterative image reconstruction,” in *Proc. IEEE Asilomar Conf. on Signals, Systems, and Computers*. IEEE, 2015.
- [7] X. Zhu and P. Milanfar, “Automatic parameter selection for denoising algorithms using a no-reference measure of image content,” *IEEE Trans. Image Processing*, vol. 19, no. 12, pp. 3116–3132, Dec. 2010.
- [8] E. C. Larson and D. M. Chandler, “Most apparent distortion: full-reference image quality assessment and the role of strategy,” *Journal of Electronic Imaging*, vol. 19, no. 1, pp. 011006–1–011006–20, 2010.
- [9] Z. Wang, A. C. Bovik, H. R. Sheikh, and E. P. Simoncelli, “Image quality assessment: from error visibility to structural similarity,” *IEEE Trans. Image Processing*, vol. 13, no. 4, pp. 600–612, Apr. 2004.
- [10] H. R. Sheikh, M. F. Sabir, and A. C. Bovik, “A statistical evaluation of recent full reference image quality assessment algorithms,” *IEEE Trans. Image Processing*, vol. 15, no. 11, pp. 3441–3451, Nov. 2006.
- [11] Z. Wang, E. P. Simoncelli, and A. C. Bovik, “Multiscale structural similarity for image quality assessment,” in *Proc. IEEE Asilomar Conf. on Signals, Systems, and Computers*, 2003, vol. 2, pp. 1398–1402.
- [12] A. P. Bradley, “A wavelet visible difference predictor,” *IEEE Trans. Image Processing*, vol. 8, no. 5, pp. 717–730, May 1999.
- [13] S. J. Daly, “Visible differences predictor: an algorithm for the assessment of image fidelity,” in *Symposium on Electronic Imaging: Science and Technology*, 1992, pp. 179–206.
- [14] Z. Wang and A. C. Bovik, “Modern image quality assessment,” in *Synthesis Lectures on Image, Video, and Multimedia Processing*, 2006, pp. 1–156.
- [15] H. R. Sheikh and A. C. Bovik, “Image information and visual quality,” *IEEE Trans. Image Processing*, vol. 15, no. 2, pp. 430–444, Feb. 2006.
- [16] Z. Wang and Q. Li, “Information content weighting for perceptual image quality assessment,” *IEEE Trans. Image Processing*, vol. 20, no. 5, pp. 1185–1198, May 2011.
- [17] A. Shnayderman, A. Gusev, and A. M. Eskicioglu, “An SVD-based grayscale image quality measure for local and global assessment,” *IEEE Trans. Image Processing*, vol. 15, no. 2, pp. 422–429, Feb. 2006.

- [18] Q. Li and Z. Wang, "Reduced-reference image quality assessment using divisive normalization-based image representation," *IEEE J. Sel. Topics Signal Processing*, vol. 3, pp. 202–211, Apr. 2009.
- [19] R. Soundararajan and A. C. Bovik, "RRED indices: Reduced reference entropic differencing for image quality assessment," *IEEE Trans. Image Processing*, vol. 21, no. 2, pp. 517–526, Feb. 2011.
- [20] Z. Wang, G. Wu, H. R. Sheikh, E. P. Simoncelli, E. Yang, and A. C. Bovik, "Quality-aware images," *IEEE Trans. Image Process*, vol. 15, no. 6, pp. 1680–1689, Jun. 2006.
- [21] A. M. Krishna and A. C. Bovik, "Blind image quality assessment: From natural scene statistics to perceptual quality," *IEEE Trans. Image Processing*, vol. 20, no. 12, pp. 3350–3364, Dec. 2011.
- [22] A. Mittal, A. K. Moorthy, and A. C. Bovik, "No-reference image quality assessment in the spatial domain," *IEEE Trans. Image Processing*, vol. 21, no. 12, pp. 4695–4708, Dec. 2012.
- [23] S. Gabarda and G. Cristbal, "Blind image quality assessment through anisotropy," *J. Opt. Soc. Am. A*, vol. 24, no. 12, pp. B42–B51, 2007.
- [24] M. A. Saad, A. C. Bovik, and C. Charrier, "A DCT statistics-based blind image quality index," in *IEEE Signal Process. Lett.*, Jun. 2010, vol. 17, pp. 583–586.
- [25] A. K. Moorthy and A. C. Bovik, "A two-step framework for constructing blind image quality indices," *IEEE Signal Process. Lett.*, vol. 17, no. 5, pp. 513–516, May. 2010.
- [26] Z. Wang, H. R. Sheikh, and A. C. Bovik, "No-reference perceptual quality assessment of JPEG compressed images," in *Proc. Int. Conf. Image Processing*, 2002, vol. 1, pp. 477–480.
- [27] J. Caviedes and F. Oberti, "A new sharpness metric based on local kurtosis, edge and energy information," *Signal Processing: Image Communication*, vol. 19, pp. 147–161, 2004.
- [28] H. R. Sheikh, A. C. Bovik, L. Cormack, and Z. Wang, "LIVE image quality assessment database release 2," 2005, <http://live.ece.utexas.edu/research/quality>.
- [29] R. L. Joshi, V.J. Crump, and T. R. Fischer, "Image subband coding using arithmetic coded trellis coded quantization," *IEEE Trans. Circuits Syst. Video Technol.*, vol. 5, pp. 515–523, Dec. 1995.
- [30] S. M. LoPresto and K. Ramchandran, "Image coding based on mixture modeling of wavelet coefficients and a fast estimation-quantization framework," *Data Compression Conference, Snowbird, UT*, pp. 221–230, Mar. 1997.
- [31] A. Liu, W. Lin, and M. Narwaria, "Image quality assessment based on gradient similarity," *IEEE Trans. Image Processing*, vol. 21, no. 4, pp. 1500–1512, Apr. 2012.
- [32] Y. Wang, Q. Zhang, and B. Li, "Structure-preserving image quality assessment," *Int. Conf. Multimedia and Expo*, pp. 1–6, 2015.
- [33] J. Shi and C. Tomasi, "Good features to track," in *Proc. IEEE Comput. Soc. Conf. Comput. Vis. Pattern Recognit.*, 1994, pp. 593–600.
- [34] Z. Hong, "Algebraic feature extraction of image for recognition," *Pattern recognition*, vol. 24, no. 3, pp. 211–219, 1991.
- [35] Z. Wang, A. C. Bovik, and B. L. Evan, "Blind measurement of blocking artifacts in images," in *Proc. Int. Conf. Image Processing*, 2000, vol. 3, pp. 981–984.
- [36] H. R. Sheikh, A. C. Bovik, and G. Veciana, "An information fidelity criterion for image quality assessment using natural scene statistics," *IEEE Trans. Image Processing*, vol. 14, no. 12, pp. 2117–2128, Dec. 2005.
- [37] S. A. Golestaneh and L. J. Karam, "Reduced-reference quality assessment based on the entropy of DNT coefficients of locally weighted gradients," in *Proc. Int. Conf. Image Processing*, 2015.
- [38] X. Li, "Blind image quality assessment," in *Proc. Int. Conf. Image Processing*, 2002, vol. 1, pp. 449–452.
- [39] A. Buades, B. Coll, and J.M. Morel, "A non local algorithm for image denoising," in *Proc. IEEE Comput. Soc. Conf. Comput. Vis. Pattern Recognit.*, 2005, vol. 2, pp. 60–65.
- [40] L. L. Thurstone, "A law of comparative judgment," *Psychological review*, pp. 273–286, 1927.
- [41] B. Peng and O. Veksler, "Parameter selection for graph cut based image segmentation," in *Proc. Br. Mach. Vis. Conf.*, 2008, pp. 16.1–16.10.
- [42] Y. Yitzhaky and E. Peli, "A method for objective edge detection evaluation and detector parameter selection," *IEEE Trans. Pattern Anal. Machine Intell.*, vol. 25, pp. 1027–1033, Aug. 2003.
- [43] M. S. C. Almeida and M. T. Figueiredo, "Parameter estimation for blind and non-blind deblurring using residual whiteness measures," *IEEE Trans. Image Processing*, vol. 22, no. 7, pp. 2751–2763, Jul. 2013.
- [44] J. L. Herraiz, M. Ieee, S. Gabarda, G. Cristobal, and S. Member, "Automatic parameter selection in PET image reconstruction based on no-reference image quality assessment," in *Nuclear Science Symposium and Medical Imaging Conference Record*, 2012, pp. 3371–3374.
- [45] D. Weller, S. Ramani, and J. A. Fessler, "Augmented Lagrangian with variable splitting for faster nonCartesian L1-SPIRiT MR image reconstruction," *IEEE Trans. Med. Imag.*, vol. 33, no. 2, pp. 351–361, Feb. 2014.
- [46] G. Demoment, "Image reconstruction and restoration: overview of common estimation structures and problems," *IEEE Trans. Acoust. Sp. Sig. Proc.*, vol. 37, no. 12, pp. 2024–2036, Dec. 1989.
- [47] T. Wiegand and B. Girod, "Lagrange multiplier selection in hybrid video coder control," in *Proc. Int. Conf. Image Processing*, 2001, vol. 3, pp. 542–545.
- [48] L. Rudin and S. Osher, "Total variation based image restoration with free local constraints," in *Proc. Int. Conf. Image Processing*, 1994, vol. 1, pp. 31–35.
- [49] T. Goldstein and S. Osher, "The split Bregman method for L1-Regularized problems," *SIAM Imaging Science*, vol. 2, pp. 323–343, Jan. 2009.
- [50] R. K. S. Kwan, A. C. Evans, and G. B. Pike, "MRI simulation-based evaluation of image-processing and classification methods," *IEEE Trans. Medical Imaging*, vol. 18, no. 11, pp. 1085–1097, 1999.
- [51] A. Buades, B. Coll, and J. M. Morel, "A review of image denoising algorithms with a new one," *Multiscale Modeling and Simulation*, vol. 4, pp. 490–530, 2005.
- [52] T. H. Cormen, C. E. Leiserson R. L. Rivest, and C. Stein, *Introduction to Algorithm*, The MIT Press, 2001.